Transportation Research Part C 104 (2019) 158–171

Contents lists available at ScienceDirect

Transportation Research Part C

journal homepage: www.elsevier.com/locate/trc

Road grade estimates for bicycle travel analysis on a street network

Omar El Masri[a], Alexander Y. Bigazzi[b,*]

[a] Department of Civil Engineering, University of British Columbia, Canada
[b] Department of Civil Engineering and School of Community and Regional Planning, University of British Columbia, 2029 – 6250 Applied Science Lane, Vancouver, BC V6T 1Z4, Canada

ARTICLE INFO

Keywords:
Road grade
Bicycles
Elevation
GPS
Digital elevation model

ABSTRACT

Road grade is a major factor influencing walking and cycling speed, energy expenditure, and travel behaviour. Bicycling research and commercial travel applications typically use digital elevation models to estimate road grades. The goal of this research is to determine the best methods of obtaining road grade data for bicycle travel analysis on an urban street network. Multiple elevation data sources are collected for eight sample locations in the city of Vancouver, Canada. Road grade extraction algorithms are applied and compared to precise ground surveying data. Estimates of cycling power and energy are used to assess the road grade accuracy in a specific analytical context. Road grades on all 35 elevated roadways of at least 30 m in the city are also characterized and classified into 3 modalities of road grade distribution. Results show that road elevations and grades extracted from raw Light Detection and Ranging (LIDAR) data are the most accurate where directly measured grades are unavailable. Interpolation of digital elevation models (DEM) and digital surface models (DSM) can provide adequate grade estimates on non-elevated roads, but are highly inaccurate on elevated structures, leading to substantial errors in cycling power and energy estimates. Short elevated network links (under 100 m) often have unimodal grade distributions which can be approximated with straight-line elevation profiles, but longer elevated structures (such as arched spans) have more grade variability. Recommendations are made for estimating grades on a network with and without LIDAR data, with the caveat that propagation of errors in grade data should be considered in walking and cycling analysis.

1. Introduction

Models of non-motorized travel rely on precise road grade information. Route choice models for pedestrians and cyclists typically include road grade information to account for the effects of hills on route preferences (Broach et al., 2012; Broach and Dill, 2016; Casello and Usyukov, 2014). Similarly, speed models require road grade information to account for the effects of hills on cycling speed (Bigazzi and Lindsey, 2018; Parkin and Rotheram, 2010; Tengattini and Bigazzi, 2017), and cycling performance models use road grade as an input to estimates of power, energy, and physical activity (Bigazzi and Figliozzi, 2015; Martin et al., 1998; Olds et al., 1995). Road grade has also been incorporated into agent-based simulations of bicycle traffic (Ziemke et al., 2017). More broadly, terrain plays a role in perceptions of cycling infrastructure quality and hence likelihood of cycling (Teschke et al., 2017; Willis et al., 2015). While road grade is also relevant in motor vehicle speed, energy, and emissions modeling, the sensitivity of pedestrians and cyclists to road grade is greater than that of motorized modes. For example, road grade differences of 2% and less

* Corresponding author.
E-mail addresses: omar.elmasri@alumni.ubc.ca (O. El Masri), alex.bigazzi@ubc.ca (A.Y. Bigazzi).

https://doi.org/10.1016/j.trc.2019.05.004
Received 20 November 2018; Received in revised form 29 April 2019; Accepted 2 May 2019
Available online 09 May 2019

have been shown to significantly influence cycling speeds (Flügel et al., 2017) and routes (Broach et al., 2012).

Most available Geographic Information Systems (GIS) datasets like street network shape files lack road grade or elevation information (Wang et al., 2017). Thus, analysis and models of non-motorized travel, as well as services for walking and cycling such as smartphone applications, must find alternative data sources for road grade. Unfortunately, there is no optimal data source, and analysts must consider trade-offs in extent, resolution, or accuracy. This study tests and compares several methods of obtaining road grade information for bicycle travel analysis on a network, with the goal of illuminating the strengths and limitations of available data sources and providing recommendations on how best to utilize them. We believe this is an important topic, given the growth in cycling infrastructure and research, and the proliferation of high-resolution cycling (horizontal) location data from GPS-based travel surveys, bikeshare systems, and smartphone applications.

1.1. Literature review

The most common elevation datasets are in the form of a square-grid Digital Elevation Model (DEM) or Digital Surface Model (DSM) (Wilson, 2012). DSM capture above-ground structures like buildings and trees, whereas DEM represent bare-earth elevation. The past two decades have seen a rapid growth in mass-produced high-resolution DEM. At the continental scale, the Shuttle Radar Topographic Mission (SRTM) developed a 3-arc-second (90 m) grid spacing DEM in 2000 which was much better than the previous 1 km spacing of the worldwide GTOPO30 DEM (Becker et al., 2009; Farr et al., 2007). However, 90 m is still insufficient resolution for estimating road grade at the scale of walking and cycling, particularly with vertical accuracy of 10 m (Rodríguez et al., 2006). The Advanced Spaceborne Thermal Emission and Reflectance Radiometer Global Digital Elevation Model (ASTER G-DEM), released in 2009, improved resolution to 1 arc-second, with accuracies of 7–20 m vertically and 30 m horizontally (compared to 16 m and 20 m, respectively, for SRTM) (Hirano et al., 2003; Nelson et al., 2009; Slater et al., 2011; Tachikawa et al., 2011; Wilson, 2012). In Canada, the 20 m Canadian DEM (Ministry of Natural Resources, Canada, 2014a) and DSM (Ministry of Natural Resources, Canada, 2014b) are also available, derived from the SRTM.

Beyond issues of resolution and accuracy, DEM lack information on elevated roads, bridges, and tunnels. Thus, studies and applications that rely on SRTM and other DEM for elevation data misrepresent road grades on elevated structures. Fig. 1 illustrates this distortion using images from Google Earth, which places elevated structures along the ground surface. Google Maps substitutes straight-line road profiles on elevated structures, which still does not represent the actual bridge surface. These issues are shared with cycling-specific applications such as Strava and RideWthGPS as well.

Some cities have undertaken remote sensing initiatives to map the built environment in three dimensions using airborne laser scanning, in which a LIDAR (Light Detection and Ranging) system is placed on an aircraft to collect elevation and surface position data (Grejner-Brzezinska, 2002). Airborne laser scanning produces a dense “cloud” of points from which the positions of both the ground and objects above it such as trees and bridges can be identified (Li et al., 2008; Zhang and Frey, 2006). LIDAR data can be used to generate DEM and DSM with grid spacing of a meter or less and with vertical accuracy of about 30 cm (Zhang et al., 2003). Unfortunately, LIDAR data are not yet available on the same spatial extent as SRTM and ASTER data.

The literature identifies many methods to calculate road grade from gridded and point elevation data sources. Wood et al. (2014) attached elevation data from the U.S. Geological Survey (USGS) 1/3-arc second DEM to two-dimensional GPS data. Elevation data were down-sampled into uniformly-spaced intervals and passed through a combined Savitzky-Golay (Savitzky and Golay, 1964) and binomial filter. Points where elevation difference exceeded a threshold were discarded and replaced with interpolated elevation values, and the filters were applied again to reduce noise. Similarly, Liu et al. (2018) used USGS datasets of 1–10 m spacing to calculate elevation profiles of roads in a GIS network. Road points were sampled on the grid spacing of the elevation data, and then the elevation profile was completed using ordinary least squares cubic regression and smoothed using cubic spline smoothing. Payne and Dror (2017) also used the 1/3-arc second DEM from the USGS to create maps with road grade information. Nodes were added to the street network at 10 m intervals and the DEM was queried at all node coordinates. Grades were calculated as the change in elevation over the change in distance along the link. Wang et al. (2017) similarly extracted Google Earth (GE) elevation data to estimate road grade.

Souleyrette et al. (2003) used a LIDAR-based DSM to estimate road grade by defining the extent of the road segment in two

Fig. 1. Illustrations of road grade distortion based on DEM (in Google Earth).

dimensions, calculating distances for LIDAR data points from and along the centerline, and estimating a regression of the grade and banking. LIDAR data in cloud point format requires a different approach from raster-based elevation data sources such as DEM and DSM. Cai and Rasdorf (2008) describe two straightforward methods for obtaining road grade from LIDAR cloud point data, which involve buffering and interpolating LIDAR data points within a distance of the road centerline. Classifying and filtering LIDAR cloud point data can improve estimates by isolating road surface observations based on intensity (Choi et al., 2007; Clode et al., 2004; Kashani et al., 2015; Li et al., 2008). Classification methods are computationally intensive, and ideally should account for confounding factors that affect intensity including reflectivity, surface characteristics, and acquisition geometry (Hu, 2003; Kashani et al., 2015).

Zhang and Frey (2006) used regression to estimate the grade of road segments from LIDAR data, with an approach practical for a large network. The method includes five steps: [1] select LIDAR data within a buffer zone for the roadway, [2] define the roadway center line, [3] compute distances, [4] segment the roadway to eliminate the effect of vertical curvature, and [5] fit a plane to the roadway surface using bivariate linear regression. Locations with voids in the LIDAR data (near bridges, overpasses, and dense vegetation) were modeled as vertical curves connecting adjacent roadway links. The LIDAR-based road grade estimates were compared with design drawing data for selected portions of the studied roadways, revealing good fits ($R^2 > 0.9$) for road grades over 1%.

Boyko and Funkhouser (2011), added elevation to a network shapefile using elevation values in LIDAR cloud point data exclusively (i.e., without relying on inference from intensity). Their approach is to develop a cardinal spline representing road elevation pinned to control vertices at 15 m along the centerline. The first step of the method is to place spline control vertices at 15 m intervals along the two-dimensional links of the network. Then, estimate the elevation of the control vertices by minimizing the weighted squared error between a spline representing the elevation profile of the road and nearby LIDAR data points:

$$E(V) = \sum_{s \in S(V)} \left(w(s) \sum_{p \in P(s)} (s_z - p_z)^2 \right)$$

where V is the set of control vertices, $S(V)$ is the Cardinal spline defined by V, s a point sampled at 1 m intervals along S, p is a LIDAR data point in the set of points $P(s)$ within 15 cm horizontally (in 2 dimensions) of s, s_z and p_z are the elevations of s and p, respectively, and $w(s)$ is a weight computed as the inverse of the variance of the LIDAR elevations in $P(s)$ (i.e., $w(s) = \frac{1}{Var(p_z)} \; \forall \; p \in P(s)$). After estimating the spline $S(V)$ from the elevations of V, the points s are snapped to the nearest LIDAR points. Finally, each point along the link is visited in sequence and the change in elevation is set to zero if the road grade exceeds 35%.

Other than remote sensing and photogrammetry, elevation and road grade can be extracted from design drawings or surveyed in the field, both of which would be prohibitively resource intensive for an entire road network (Zhang and Frey, 2006). Design drawings may also not represent the as-built roadway. Highway grades have also been estimated using GPS (Global Positioning System) data on probe vehicles with some success, although this approach is also resource intensive because it requires sampling the entire network, and has limited accuracy (Hughes, 2014; Kim et al., 2013; Sahlholm and Henrik Johansson, 2010; Wood et al., 2014). In addition, the GPS methods have not been validated for bicycle-based data collection, which would be necessary to measure grades on a bicycle network.

1.2. Objective

The objective of this research is to determine the most appropriate methods of obtaining road grade information for modeling or analyzing cycling on a network. The specific application of interest is attaching elevation and grade information to observed GPS tracks or a sequence of links forming a route in a street network. The scope of investigation is only vertical position – it is assumed that horizontal positioning is known from GPS or GIS data. Several common sources of elevation data are compared with ground surveying data in Vancouver, Canada for accuracy of elevation and road grade. The accuracy of the methods is also compared based on estimates of cyclist power and energy expenditure, an application which is highly sensitive to road grade. Based on the results, detailed recommendations are provided for which data sources to use for road grade estimates on elevated and non-elevated links in a network.

2. Method

2.1. Elevation data sources

The elevation data sources investigated in this study for Vancouver, Canada are summarized in Table 1 (all open data). LIDAR cloud point data were provided by the City of Vancouver, collected over three days in February 2013 (The City of Vancouver, 2013). The City used the LIDAR cloud point data to create a 0.5 m DEM raster, publicly available online, from ground-classified points using a binning approach: averaging the filtered points within each cell of the raster, with linear interpolation for hole-filling. A 0.5 m DSM raster was similarly created from first returns. The original classified LIDAR cloud point data were also obtained from the City for use in this study.

The Canadian DEM is based on the elevation contours and hydrographic data of Natural Resources Canada's (NRCan) Geospatial Data Base at the scale of 1:50000, as well as data at various scales provided by provinces and territories. The Canadian Digital Surface Model (CDSM) was derived from the SRTM in 2010 (Ministry of Natural Resources, Canada, 2014a). Original SRTM elevation data at

Table 1
Elevation data sources compared in this study.

Name	Format and grid Spacing[a]		Extent	Base Data	Reported Accuracy
LIDAR cloud point	Cloud points		City of Vancouver	Vancouver LIDAR (2013)	≤1 m
Vancouver DEM	Raster:	0.5 m	City of Vancouver	Vancouver LIDAR (2013)	≤1 m
Vancouver DSM	Raster:	0.5 m	City of Vancouver	Vancouver LIDAR (2013)	≤1 m
Canadian DEM	Raster:	~20 m	Canada	Natural Resources Canada Geospatial Database	Not Available
Canadian DSM	Raster:	~20 m	Canada	SRTM	10–20 m
SRTM 1arcs DEM	Raster:	~30 m	80% of world	SRTM	10–20 m
ASTER DEM	Raster:	~30 m	99% of world	ASTER	10–50 m
SRTM 3arcs DEM	Raster:	~90 m	80% of world	SRTM	10–20 m
CGIAR SRTM DEM	Raster:	~90 m	80% of world	SRTM	10–20 m

[a] ~ 20, ~30, and ~ 90 m are 0.75, 1, and 3 arc seconds, respectively.

one arc second step were reprocessed at a grid resolution of 0.75 arc seconds, the vertical datum changed, gaps filled, water surfaces leveled, and then filtered for noise.

Four versions of the SRTM and ASTER global DEM datasets were compared with the more local elevation data sources. The joint Japanese-US ASTER G-DEM version 2 (latest version), released in 2011 with a resolution of 1 arc second, was used, as well as version 2.1 of the SRTM, released in 2009 with a resolution of 3 arc seconds, and a resampled 1 arc second version released in 2014 (Jarihani et al., 2015). The Consortium for Spatial Information of the Consultative Group of International Agricultural Research (CGIAR-CSI) further processed the SRTM data to create a version (4.1) with better quality control and 3 arc second resolution, which was also included (Jarvis et al., 2008).

The data sources summarized in Table 1 are those available for the study area and compared in the analysis. Large-scale DEM are available for other countries at different resolutions. The U.S. Geological Survey, for example, maintains an open National Elevation Dataset at 1/3 arc second (approximately 10 m), with resolutions as high as 1 m available for some areas (U.S. Geological Survey, 2015). A pan-European DEM is available at 1 arc second (approximately 30 m) (DHI GRAS, 2014), but higher resolutions are available for individual countries. The UK, for example, has released a LIDAR-based DSM of 50 cm (UK Environment Agency, 2019).

2.2. Ground truth data collection

Ground truth road grades were measured to evaluate the nine data sources. Eight sample locations in the City of Vancouver were selected to represent a variety of facility types, surrounding land use, and grades, as summarized in Table 2. The locations had to be part of the cycle network and have a Vancouver Surveying Monument (Altenhoff, 2017) nearby to allow for correct elevation referencing. Three of the locations were elevated structures: one bridge over land (Main Street Bridge), one over water (Burrard Bridge), and a two-story spiral ramp for pedestrians and cyclists connecting to the north end of the Cambie Bridge deck (Cambie Bridge North Ramp). Two locations were under a bridge: one on a local street (Beach Street) and one on an off-street path (Island Park Walk). The other three locations were not on or under an elevated structure: one in the downtown core surrounded by tall buildings (Smithe Street), and two in a mid-rise residential area, one flat (West 10th Street) and one on a hill (Trafalgar Street). The sampling locations are shown on a map in Supplemental Material, Fig. S1.

Elevation measurements along the sampled facilities were made using a Leica TCR700 total station, with an angle accuracy of 5 s and a distance accuracy of 3 mm, and a standard reflector prism. At each site, elevations were measured from the closest surveying monument, and the total station was relocated when the target prism was occluded or farther than 100 m. Measurements were made at predetermined intervals along the road at a fixed distance parallel to the curb using measuring tape. Measurements were made in the path for off-street and separated cycle facilities and on the road for shared on-street facilities. The sampling interval was 5 m for locations up to 300 m in length and 10 m otherwise due to time constraints. Six measurements were taken at each sample and the average used as the ground truth. The standard deviation of the measurements at each sample had a maximum value of 6 mm and an average of 1 mm, indicating high precision in the ground truth measurements.

2.3. Road grade estimation from elevation

Two methods are used to estimate road grade from DEM and DSM datasets. In the first method, elevation values are simply extracted from the raster cells corresponding to points of interest (i.e., sampling points along a network link at 5 m or 10 m intervals). The second method uses bilinear interpolation (Press, 1992) to estimate elevation values at each point based on the four nearest raster cells, rather than simple extraction from a single cell. In both methods, road grade is calculated from points along a link as the ratio of first differences of elevation and horizontal position between consecutive points. Fig. 2 illustrates the difference between the two methods using the Canadian DSM at Smithe Street.

The method of Boyko and Funkhouser (2011), described in the Introduction, was applied to estimate road grades from the LIDAR cloud point data. Because some studies and applications like Google Maps use a straight-line approximation for the elevation profile of elevated structures or links with missing information, a straight-line (constant grade) elevation profile between ground-measured endpoints was also used as a comparison case.

Table 2
Ground truth sample locations.

Location Name	Description	Bicycle facility	Elevated	Under a Bridge	Sampled length (m)	Sampling interval (m)	Sample points
West 10th Street	Flat low-volume street in mid-rise residential area	Shared local street in bicycle network	No	No	120	5	25
Trafalgar Street	Steep low-volume street in mid-rise residential area	Shared local street in bicycle network	No	No	60	5	13
Smithe Street	Steep street in downtown	On-street separated cycle track	No	No	75	5	16
Beach Street	Low-traffic street under bridge in downtown	Shared local street in bicycle network	No	Yes	90	5	19
Island Park Walk	Flat off-street path in treed area under a bridge	Off-street paved cycle path	No	Yes	75	5	16
Main Street Bridge	Moderately graded bridge crossing railroad tracks	Shared local street	Yes	No	255	5	52
Burrard Bridge	Long, moderately graded bridge crossing water	On-street separated cycle track	Yes	No	1010	10	102
Cambie Bridge North Ramp	Two-story spiral ramp connecting the ground to the bridge deck	Off-street paved shared pedestrian and cycle path	Yes	No	135	5	28

2.4. Performance measures

The elevation profiles and road grades were evaluated based on several measures, each calculated at the sampling interval for the location (every 5 or 10 m along the facility). Elevation and grade accuracy were assessed using mean and standard deviation of absolute error (compared to ground truth) and Pearson correlation coefficients. Grade distributions were also compared using the coincidence ratio (the ratio of the intersection of two distributions to the union of the two distributions), calculated at 1% grade intervals. Coincidence ratio values range from 0 to 1, with higher values indicating greater alignment.

To provide a cycling-specific context to evaluate the accuracy of the datasets and methods, cycling power required to traverse each facility in the uphill direction was estimated and compared. Power P in Watts was estimated using: $P = mg(C_r + G)v + 0.5\rho C_d A_f v^3$ (Bigazzi and Figliozzi, 2015), where mg is the total weight (N) of the cyclist, bicycle, and cargo, C_r (unit-less) is the rolling resistance coefficient, G is road grade (unit-less), v is speed relative to wind (m/s), ρ is air density (assumed 1.225 kg/m^3), and $C_d A_f$ is the effective frontal area (m^2). Assumed values of $C_r = 0.0077$, $C_d A_f = 0.559\text{m}^2$, and mg = 105 kg for urban cyclists in Vancouver were taken from Tengattini and Bigazzi (2018). Speed v was assumed to be a constant representative value of 4 m/s (14 km/h), based on Bernardi and Rupi (2015). In addition to power, cyclist energy output E to traverse each interval of length L (5 or 10 m) was calculated as $E = P\frac{L}{v}$ (in Joules) and summed to estimate total energy for each facility.

2.5. Characterization of elevated road structures

Because of a particular interest in elevated road structures (which are not represented in DEM), further work was done to characterize grades on the structures within the City of Vancouver (the spatial extent of the LIDAR cloud point data). Elevated structures of at least 30 m in length were identified based on a binary elevated attribute for links in Open Street Maps (OSM) network data (OpenStreetMap contributors, 2017). After removing duplicates (due to multiple facilities on the same bridge deck, for example), 35 elevated road structures of at least 30 m were identified within the City.

The elevation profiles for these structures were extracted from the LIDAR cloud point data using the same method as above. The structures were then classified based on the modality of their road grade distributions. Modality was determined using Kernel Density Estimates (KDE) (Hall and York, 2001; Ling et al., 2014) with a bandwidth of 0.5%, with modes identified at local maxima (Silverman, 1981). Unimodal structures were fitted with a parametric distribution using maximum likelihood estimation (Scholz, 2006).

3. Results

3.1. Elevation profiles

Fig. 3 gives the elevation profiles of Trafalgar Street from the eight DEM and DSM elevation sources, with and without interpolation, along with the measured ground truth elevation profile. The high-resolution Vancouver DEM provides a close match to the measured road grade, while the Vancouver DSM is several meters above the road surface in two locations (with trees over the road). The other DEM and DSM based on SRTM or ASTER data are clearly too coarse to represent the grade of this section of road without interpolation. The 30–90 m grid spacing provides only 1–3 unique elevation values over the 60 m road section, which leads to

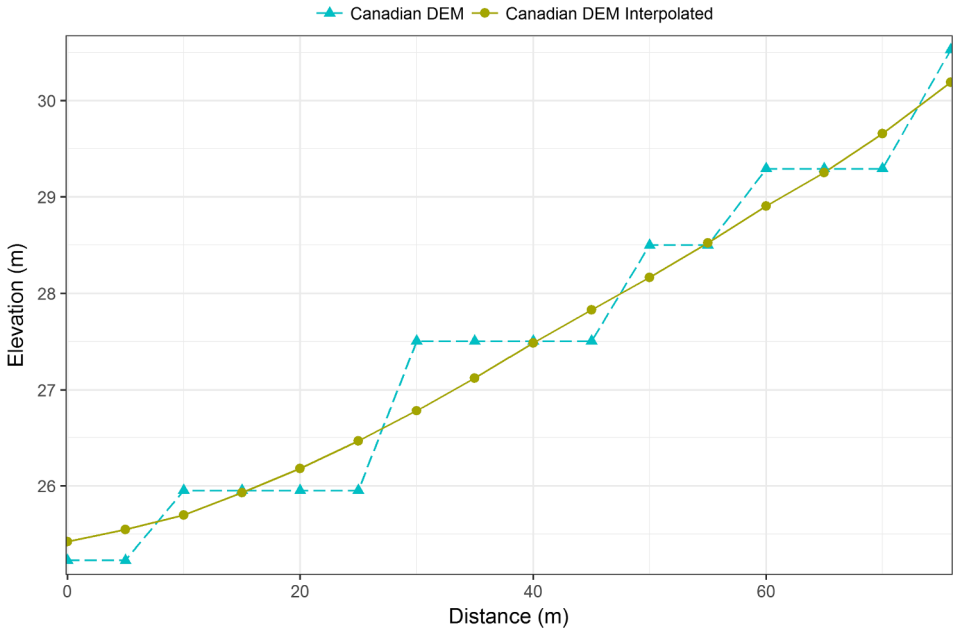

Fig. 2. Elevation profile of Smithe Street location based on the Canadian DSM using simple extraction and bilinear interpolation.

alternating flat and steep intervals without interpolation. The absolute elevation values of the coarse DEM and DSM are inaccurate as well, with as much as 8 m difference from measured road grade (as expected from Table 1). Similar results were obtained from non-interpolated DEM/DSM data at the other locations. For the rest of the paper, only DEM/DSM results using bilinear interpolation are presented.

Fig. 4 gives the elevation profiles of Smithe Street and Beach Street for the best-performing DEM/DSM in Fig. 3 (the LIDAR-derived Vancouver DEM and Vancouver DSM), LIDAR cloud point data (based on the Boyko method), and ground truth measurement. Again, the Vancouver DSM is heavily influenced by objects over the road (trees on Smithe Street and the Burrard Bridge deck on Beach Street), leading to large errors in elevation and grade. The elevation profile extracted from the LIDAR cloud point data is also influenced by the above-ground LIDAR returns, which leads to smaller inaccuracies. The Vancouver DEM closely tracks the grade of the measured ground truth, although there is a small vertical offset which could be due to a datum error. The elevation profiles for these two locations including interpolated values from the other DEM are given in Figs. S5 and S6; even with interpolation, the low resolution and precision of the other DEM lead to large inaccuracies. Elevation profiles for all locations are given in the Supplemental

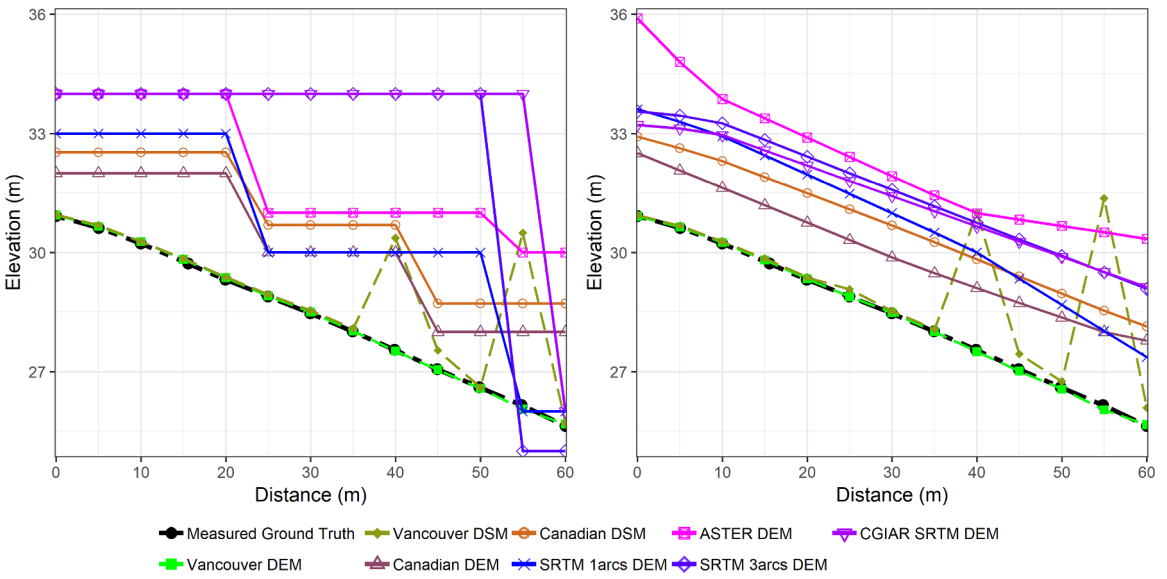

Fig. 3. Elevation profiles of Trafalgar Street, without (left) and with (right) interpolation of DEM/DSM.

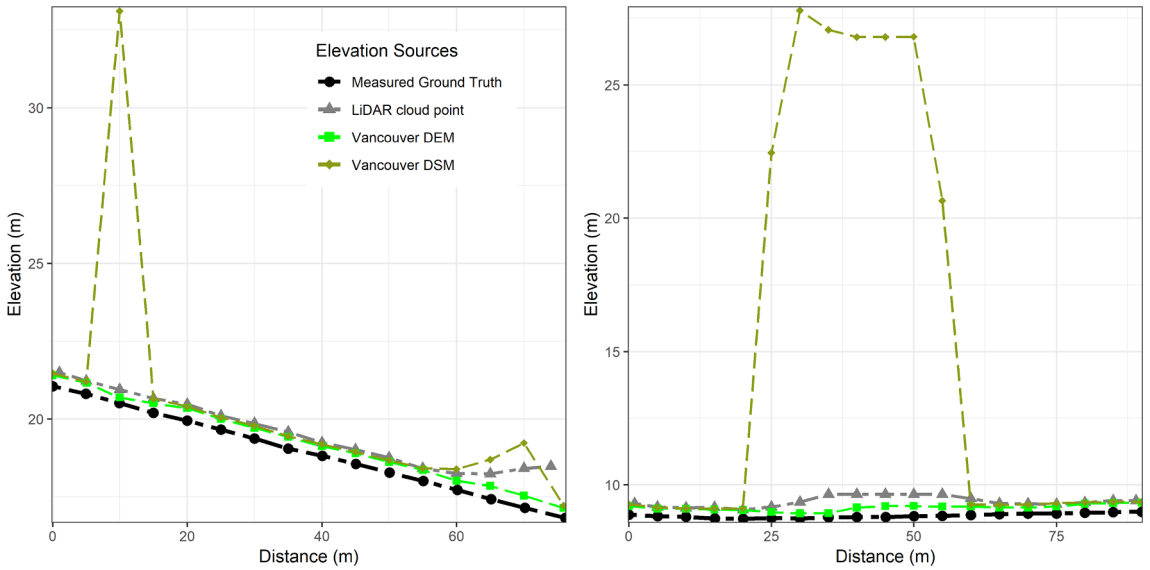

Fig. 4. Elevation profiles of Smithe (left) and Beach (right) Streets, from LIDAR-derived data sources.

Material.

Fig. 5 gives elevation profiles for the Burrard Bridge from all nine data sources and the ground truth measurements. The DEM all represent the water or ground surface below the bridge deck, leading to large errors in the elevation profile. The high-resolution Vancouver DSM generally follows the bridge deck, but provides erroneous values at the crest of the bridge where there is a superstructure over the deck. Only the processed LIDAR cloud point data track the bridge deck closely throughout the span. As further validation, the Burrard Bridge design drawings were obtained from the City of Vancouver, which identify the grade as +3% and −3% on the two main graded sections of the bridge (connected by a crest vertical curve). In comparison, the LIDAR cloud point method generated average road grade estimates of 3.03% (standard deviation 0.69%) and –2.90% (standard deviation 0.53%) for those sections of the bridge.

Fig. 6 gives the elevation profiles of the Cambie Bridge North Ramp. All the data sources fail to accurately represent the elevation profile of this unique facility. The Vancouver DSM comes closest on the exposed second half of the ramp, but is inaccurate before that, tracking only the upper level of the two-level spiral ramp. The processed LIDAR cloud point data fails to follow the ramp surface, likely because of the wide vertical distribution of LIDAR returns (the Boyko method reverts to zero grade if the change in elevation

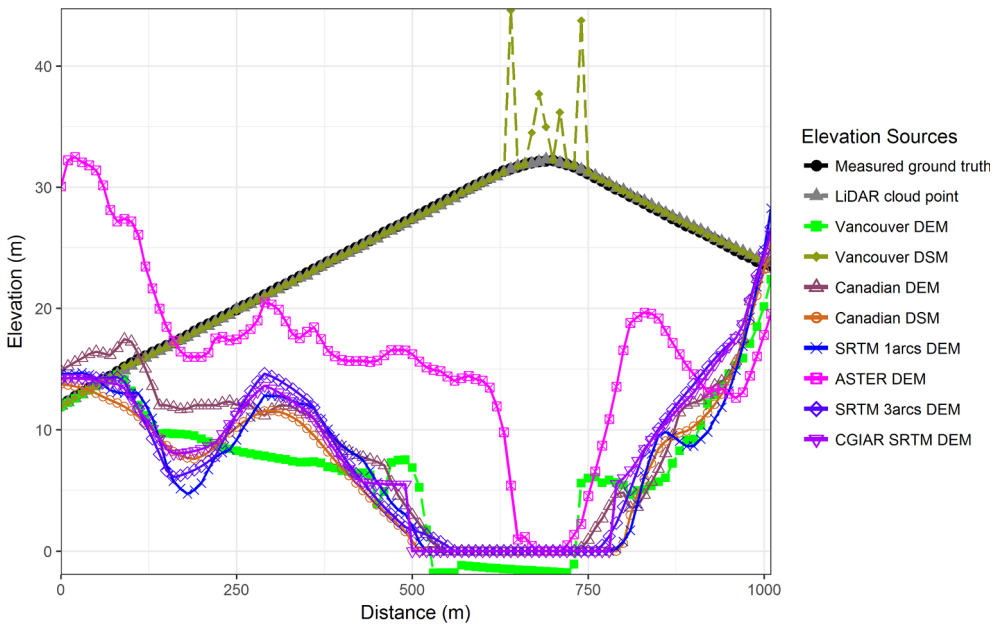

Fig. 5. Elevation profiles of Burrard Bridge from all sources.

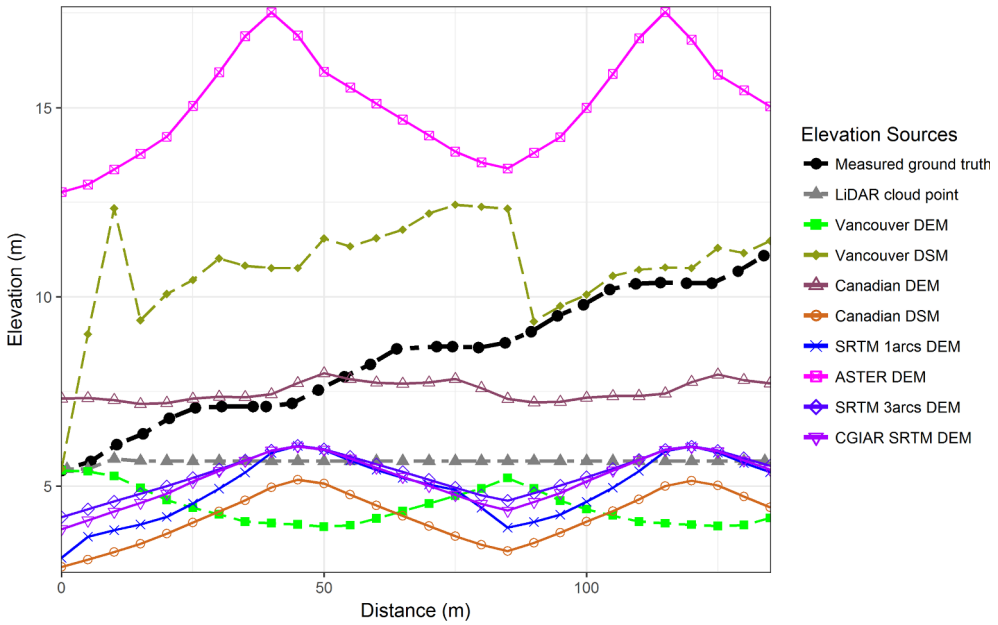

Fig. 6. Elevation profiles of Cambie Street North Ramp from all sources.

Table 3
Mean (standard deviation) absolute error in elevation (m) at each location.

Data Source	West 10th Street	Trafalgar Street	Smithe Street	Beach Street	Island Park Walk	Main Street Bridge	Burrard Bridge	Cambie Bridge North Ramp
Straight-line	0.19 (0.11)	0.12 (0.07)	0.01 (0.01)	0.09 (0.06)	0.47 (0.30)	3.41 (2.12)	6.58 (3.78)	0.21 (0.16)
LIDAR cloud point	0.40 (0.12)	0.13 (0.07)	0.61 (0.35)	0.53 (0.21)	0.39 (0.25)	0.27 (0.13)	0.13 (0.05)	2.74 (1.62)
Vancouver DEM	0.29 (0.11)	0.04 (0.03)	0.34 (0.06)	0.30 (0.07)	0.38 (0.32)	3.39 (3.93)	17.29 (10.49)	3.94 (1.93)
Vancouver DSM	5.82 (5.25)	0.79 (1.62)	1.34 (3.04)	6.39 (8.25)	9.71 (11.98)	0.23 (0.12)	0.50 (1.89)	2.39 (1.74)
Canadian DEM	1.82 (0.26)	1.59 (0.22)	3.49 (0.30)	3.44 (0.35)	7.38 (2.31)	2.54 (1.53)	16.19 (10.75)	1.44 (1.04)
Canadian DSM	3.69 (0.40)	2.23 (0.14)	8.49 (2.87)	2.65 (2.24)	4.58 (0.68)	4.69 (2.16)	17.36 (10.57)	4.20 (1.47)
SRTM 1arcs DEM	4.40 (0.63)	2.42 (0.33)	10.18 (6.14)	4.62 (2.71)	6.35 (1.29)	4.19 (1.90)	17.26 (10.48)	3.45 (1.44)
ASTER DEM	9.99 (2.05)	3.91 (0.51)	0.74 (0.51)	5.17 (1.55)	9.08 (0.99)	2.79 (1.62)	12.39 (8.63)	6.70 (1.73)
SRTM 3arcs DEM	3.66 (0.28)	3.13 (0.21)	7.79 (3.44)	5.67 (2.87)	5.31 (0.75)	4.30 (2.08)	16.46 (10.72)	3.06 (1.47)
CGIAR SRTM DEM	3.34 (0.79)	2.97 (0.33)	8.09 (2.38)	4.75 (1.92)	5.42 (0.72)	3.86 (2.01)	16.37 (10.68)	3.19 (1.46)

exceeds 35%). Road grade estimates resulting from the measured and estimated elevation profiles at all eight locations are given in the Supplemental Material, along with the complete elevation profiles. Summary statistics for the measured grades are given in Table S1, with a range of − 10% to + 12%.

3.2. Elevation and grade accuracy

Table 3 gives the mean and standard deviation of absolute error in elevation compared to ground truth at each location (with 13–102 sample points per location – see Table 2). On non-elevated roads (the first five locations in the table), the Vancouver DEM, LIDAR cloud point, and straight-line estimates consistently provide the least-error elevation profiles (all with mean absolute error under 1 m). On the two arched elevated structures (Main Street and Burrard Bridges) the LIDAR cloud point and Vancouver DSM data provide the least-error elevation profiles, and on the Cambie Bridge North Ramp the straight-line estimates are least-error. No data source provides low-error elevation profiles for all 8 locations, but the 3 LIDAR-derived data sources are generally most accurate.

Table 4 gives the mean and standard deviation of absolute error in grade compared to ground truth at each location. The grade results are more varied than the elevation accuracy given in Table 1. The straight-line estimates are accurate for the non-elevated roads, but they require accurate knowledge of the endpoint elevations, and are only accurate in locations with low standard deviation in grades (see Table S1). The LIDAR cloud point data provide the most reliable grade estimates across all locations, with mean absolute error under 5%. Grades based on the Vancouver DEM are accurate on non-elevated roads. Grades from the Vancouver DSM are highly inaccurate in most locations despite moderately good elevation accuracy in Table 3. The high-resolution DSM elevations are more variable than the other data sources (note the high standard deviations in Table 3), leading to larger grade estimation errors. The Vancouver DSM provides highly accurate grade estimates on the Main Street Bridge (with no superstructure), but not the Burrard Bridge (which has a superstructure). The coarse DEM and DSM generate grades of inconsistent accuracy, sometimes better than the

Table 4
Mean (standard deviation) absolute error in grade (%) at each location.

Data Source	West 10th Street		Trafalgar Street		Smithe Street		Beach Street		Island Park Walk		Main Street Bridge		Burrard Bridge		Cambie Bridge North Ramp	
Straight-line	0.6	(0.5)	0.7	(0.8)	0.4	(0.3)	0.4	(0.4)	2.7	(1.2)	4.9	(3.3)	2.5	(1.1)	3.1	(1.3)
LIDAR cloud point	1.1	(0.6)	1.2	(1.0)	2.5	(2.7)	1.6	(1.6)	1.9	(1.7)	1.4	(1.0)	0.5	(0.4)	4.1	(3.2)
Vancouver DEM	1.0	(0.7)	0.6	(0.8)	1.2	(1.0)	0.9	(0.9)	4.5	(6.1)	7.7	(12.8)	7.4	(9.5)	6.2	(4.3)
Vancouver DSM	107.2	(95.5)	28.2	(40.8)	36.9	(84.3)	41.8	(83.6)	65.4	(154.1)	0.8	(0.6)	7.3	(25.7)	12.9	(22.0)
Canadian DEM	2.0	(1.0)	1.6	(1.6)	2.0	(1.1)	2.7	(1.3)	29.1	(24.8)	7.6	(7.5)	7.0	(6.0)	5.3	(3.4)
Canadian DSM	1.4	(0.7)	0.8	(0.6)	11.8	(1.9)	8.4	(2.5)	5.0	(3.4)	5.9	(4.2)	7.0	(5.7)	5.5	(4.3)
SRTM 1arcs DEM	2.6	(1.1)	1.7	(1.5)	22.9	(9.2)	17.1	(7.8)	6.2	(2.6)	7.4	(5.1)	8.1	(7.6)	6.6	(4.2)
ASTER DEM	5.2	(4.3)	4.7	(4.9)	5.2	(3.4)	4.9	(2.7)	6.6	(4.5)	7.0	(5.7)	9.6	(9.4)	10.9	(6.8)
SRTM 3arcs DEM	1.5	(1.3)	1.3	(1.3)	13.7	(3.8)	10.1	(1.5)	4.6	(2.5)	6.5	(4.6)	7.9	(5.5)	4.9	(3.6)
CGIAR SRTM DEM	1.9	(1.0)	2.0	(1.2)	9.6	(1.7)	6.8	(1.2)	4.9	(3.7)	6.5	(4.7)	7.4	(8.7)	5.0	(4.0)

Table 5
Coincidence ratios of grade distributions compared to ground truth.

Data Source	West 10th Street	Trafalgar Street	Smithe Street	Beach Street	Island Park Walk	Main Street Bridge	Burrard Bridge	Cambie Bridge North Ramp
Straight-line	0.17	0.09	0.58	0.57	0.00	0.01	0.02	0.02
LIDAR cloud point	0.50	0.41	0.36	0.20	0.30	0.52	0.74	0.15
Vancouver DEM	0.55	0.71	0.43	0.57	0.36	0.42	0.16	0.23
Vancouver DSM	0.09	0.33	0.36	0.44	0.50	0.52	0.63	0.26
Canadian DEM	0.17	0.14	0.20	0.13	0.07	0.31	0.17	0.29
Canadian DSM	0.33	0.20	0.00	0.00	0.20	0.36	0.14	0.23
SRTM 1arcs DEM	0.02	0.41	0.00	0.03	0.15	0.33	0.10	0.20
ASTER DEM	0.12	0.33	0.11	0.06	0.11	0.23	0.16	0.13
SRTM 3arcs DEM	0.37	0.09	0.00	0.00	0.15	0.40	0.10	0.13
CGIAR SRTM DEM	0.23	0.04	0.00	0.00	0.11	0.40	0.08	0.20

Table 6
Total cycling energy (kJ) calculated from each elevation data source.

Data Source	West 10th Street	Trafalgar Street	Smithe Street	Beach Street	Island Park Walk	Main Street Bridge	Burrard Bridge	Cambie Bridge North Ramp
Measured Ground Truth	5.1	6.1	5.3	1.1	2.8	11.9	13.3	0.6
Straight-line	5.1	6.2	5.3	1.1	2.8	7.7	1.7	0.0
LIDAR cloud point	5.3	6.1	4.3	1.5	2.3	11.9	13.2	1.8
Vancouver DEM	5.3	6.2	5.3	1.3	3.6	15.2	31.6	4.1
Vancouver DSM	74.3	13.4	18.0	20.2	27.4	11.9	48.3	7.6
Canadian DEM	4.8	5.7	4.4	2.1	14.6	12.1	29.4	2.4
Canadian DSM	4.1	5.7	0.0	0.3	3.5	11.1	27.5	3.4
SRTM 1arcs DEM	3.8	7.2	0.0	0.4	6.3	13.1	34.1	3.7
ASTER DEM	3.5	6.5	6.2	5.5	5.6	14.6	57.2	7.7
SRTM 3arcs DEM	3.9	5.4	0.0	0.0	4.2	11.8	31.9	2.8
CGIAR SRTM DEM	3.1	5.0	0.0	0.0	1.9	11.8	29.3	3.1

Table 7
Classification summary of elevated roads in the City of Vancouver.

Parameters[a]	Class 1 (unimodal, N = 13)	Class 2 (bimodal, N = 9)	Class 3 (3 + modes, N = 13)
Length (m)	63.0 (16.5)	517.3 (356.9)	482.2 (565.3)
Absolute elevation change (m)	1.1 (0.9)	5.9 (5.4)	3.6 (2.7)
Cumulative elevation gain (m)	0.9 (1.0)	3.0 (5.7)	6.3 (7.3)
Cumulative elevation loss (m)	0.2 (0.4)	6.0 (5.4)	5.9 (7.0)
Absolute average grade (%)	1.7 (1.2)	1.0 (0.6)	1.6 (1.3)
Standard deviation grade (%)	0.4 (0.3)	1.6 (0.6)	3.1 (1.4)

[a] Mean (standard deviation) by location.

elevation accuracy if they follow the general grade trend but at an offset.

Table 5 gives the coincidence ratios of the grade distributions for each location and data source compared to ground truth. The grade distribution results are slightly different from Table 4. While the straight-line estimates provide low mean absolute error, in most locations they do not represent the grade distribution as well as the LIDAR-derived data sources, which have higher coincidence ratios. Again, no data source provides the most accurate grade distribution estimates across all eight locations.

Table 6 gives the calculated cycling energy expenditure required to traverse each location, based on grade estimates from each elevation data source (and all other factors equal). The large grade errors from the Vancouver DSM (seen in Table 4) lead to large errors in calculated cycling energy, which are an order of magnitude higher than those based on measured grade for all the non-elevated roads. The LIDAR cloud point-based energy estimates are most consistently close across all locations, notably on the two arched spans; no other elevation data source is within 80% of the measured-grade-based energy values. Corresponding average power estimates are given in Table S2, with the same pattern of accuracy across locations/data sources, but in addition showing that the inaccurate grade sources generate unrealistic power estimates (over 900 W in some instances).

3.3. Characterization of elevated structures

The preceding results illustrate the challenge of estimating road grades on elevated structures without LIDAR cloud point data. The 35 elevated road structures of at least 30 m in the City of Vancouver are summarized in Table 7, based on the LIDAR cloud-point data. Thirteen locations have unimodal grade distributions (Class 1), 9 locations have bimodal grade distributions (Class 2) and 13

Table 8
Road grade (%) distribution characteristics of Class 2 bimodal elevated structures.

Location	Median	Mean	Standard deviation	Range		First mode	Second mode	Mode Spacing
1	−0.54	−0.68	0.88	(−3.92;	1.58)	−3.17	−0.52	2.66
2	−0.44	−1.39	2.12	(−4.85;	1.13)	−3.91	0.63	4.54
3	−0.24	−0.64	0.81	(−2.31;	0.11)	−2.03	−0.20	1.83
4	−1.21	−1.94	1.70	(−5.59;	2.01)	−4.39	−0.99	3.40
5	−1.06	−1.59	1.42	(−5.71;	1.77)	−4.79	−0.94	3.86
6	0.45	−0.15	2.10	(−5.04;	2.93)	−3.62	0.78	4.40
7	−0.76	−1.24	1.22	(−3.72;	0.05)	−3.38	−0.52	2.86
8	0.90	0.59	1.44	(−3.82;	4.48)	−1.81	1.09	2.90
9	2.80	0.99	2.65	(−3.39;	3.92)	−2.98	2.95	5.93

locations have grade distributions of three or more modes (Class 3). Five of the structures cross a body of water, 1 in Class 2 and 4 in Class 3 (none in Class 1). The Class 1 unimodal locations with a single consistent grade are much shorter than the other two classes, with a consistently small net elevation change and moderate grade. These are short bridges over rail or road cuts. The Class 2 locations are longer arched spans with greater net elevation changes and a wider range of grades, but still dominated by a single up and single down grade; Class 3 locations are also long, but with a wider variety in grades.

For locations without LIDAR cloud point data, the grade distributions of Class 1 unimodal elevated structures can be approximated as a normal distribution centered on the mean grade (which can be inferred from the elevation of the endpoints), and assuming a representative standard deviation (i.e., 0.42% from Table 7). Such an approximation could be used in situations where the grade sequence is not necessary, such as the cycling power model applied in this study. Class 2 bimodal locations have two dominant grades connected by a short vertical curve (such as the Burrard Bridge). The distribution characteristics of the nine bimodal locations are summarized in Table 8. The two modes lie on either side of the mean grade, separated by a spacing of 1.8–4.5% difference in grades. Half the locations have an upward and a downward mode, whereas the other half have two dominant grades in the same direction. The two modes are not consistently symmetrically spaced around the median or mean grade, due to differences in the length of each mode. An inspection of the 13 Class 3 structures reveals even more variability (Table 7), with elevation profiles composed of 3 or more single-grade segments or of a wide vertical curvature that spans a range of grades.

4. Discussion

The results show that road grades derived from LIDAR cloud point data are generally most accurate where directly measured grades are unavailable. High-resolution, LIDAR-derived DEM provide good grade estimates on non-elevated roads, but not elevated roads. High-resolution, LIDAR-derived DSM provide accurate grade estimates on elevated roads without a superstructure but can be highly inaccurate in other locations. Grades interpolated from the coarser DEM and DSM provide moderately accurate approximations for non-elevated roads with consistent grades, but poor estimates otherwise. In short, commonly-used DEM and DSM provide poor road grade estimates in some locations for active travel applications.

The distinct performance on elevated versus non-elevated roads of different data sources is important. Even as high-resolution DEM become more broadly available for road grade estimates, the problem of elevated structures will persist. Without LIDAR cloud point data, there is no clear method to obtain accurate road grades on elevated structures. Short structures under about 100 m can reasonably be assumed to be unimodal and approximated with a straight-line or normal distribution (Table 7). But longer structures have large variability in grade distributions, often multi-modal, which are poorly represented by linear approximations.

In recent work, Liu et al. (2018) generated road grade estimates for local roads and highways with root mean square error (RMSE) of $< 1\%$ compared to measured data at 7 locations in Georgia, USA. The lower error in that study can be attributed to a dominance of non-elevated locations in the validation data set, for which DEM are generally representative. The approach required a partially manual removal of “erroneous” data, presumably due to “elevated roadways and bridges”; it is unclear how many erroneous data were imputed or “filled”, but the figures suggest less than 5%. If the elevated structures included in the study were short and unimodal (Class 1 in this paper), an imputation or “hole-filling” approach is likely more accurate than for higher-modal structures (i.e., arched spans). Thus, broad scale DEM with a filter for elevated structures and imputation/smoothing technique can be accurate over most of the network, but will fail on larger and complex elevated structures such as arched spans.

The question then becomes – how important are these isolated errors on elevated structures? As noted above, there are only 35 elevated road structures of over 30 m in the City of Vancouver, which is a small portion of the entire road network. There would likely be more in cities with urban freeways or more surface water bodies (such as canals), but it would still likely be a small share. On the other hand, these crossings tend to be high-volume facilities, because they are critical links in the network. Bridges are often primary targets for bicycle infrastructure, for example. Accurate grade data for bridges is important for bicycle and pedestrian analysis that includes energy expenditure, travel time, or air pollution inhalation. Accurate road grades are also important for active travel behaviour modeling that includes hills as an independent variable (i.e., route choice models).

Based on the results presented above, the following approach is recommend for future active travel studies or routing/mapping applications requiring network-wide road grade information. The recommendation assumes use of Open Street Maps or similar network data in which a flag is available to identify links that are elevated.

- If LIDAR cloud-point data are available,
  - o on non-elevated links use a last-return-based high-resolution DEM to estimate grades, and
  - o on elevated links use a cloud-point processing algorithm such as Boyko and Funkhouser (2011) to estimate grades.
- If LIDAR cloud-point data are not available,
  - o on non-elevated links use the highest-resolution DEM available to estimate grades with a smoothing/interpolation filter,
  - o on elevated links of length up to 100 m, estimate grades by imputing between the nearest non-elevated nodes (a constant-grade assumption), and
  - o on elevated links of over 100 m seek out alternative data sources such as design drawings.

The recommendation to seek out alternative data sources for elevated links of over 100 m without LIDAR cloud point data is unsatisfying, but the results above show that DEM of any resolution are highly inaccurate for these structures. Also, design drawings are more likely to be available for significant infrastructure such as arched spans. If long spans are central to the analysis network, such as the Burrard Bridge in Vancouver, special effort is warranted to seek out design drawings or even undertake ground surveying. As a last resort, a straight-line constant-grade approximation is still likely better than DEM-based grade estimates for long elevated spans.

One potential approach to estimating grades on long spans is inference from GPS data. Typical consumer-grade GPS devices (such as smartphones) may not provide accurate elevation data, but statistical methods (such as used here with LIDAR cloud-point data) could be applied to large, crowd-sourced GPS datasets to infer road grade. Obtaining disaggregate GPS data in sufficient volume is the largest obstacle to this approach, but it could be undertaken by smartphone location data aggregators. On the other hand, much less GPS data would be required to infer grades from GPS devices with higher accuracy, such as the instruments used in Boriboonsomsin and Barth (2009). This type of instrumentation is more difficult to apply on a bicycle network, but an instrumented bicycle could be developed for such a purpose.

In all cases, the limitations of using LIDAR or DEM to generate road grades should be understood and considered in analysis. Physiological or behavioural models of speed, route, or energy during walking and cycling should consider how grade errors propagate through the models. As shown in Table 6, for locations such as the Burrard Bridge, elevation data sources other than LIDAR cloud-point data generate cyclist energy estimates off by a factor of 2 or more.

The importance of accurate road grade data for the transportation field is expected to increase with the advancement of new technologies and data streams. For example, smartphone-derived GPS data are increasingly used for travel surveys (Gadziński, 2018) and routing models (Oyama and Hato, 2018), among other applications. But there are still challenges to processing and application of these GPS data, including inference of travel modes (Huang et al., 2019) and map matching (Knapen et al., 2018). More accurate road grade information could be used to improve the performance of existing algorithms, since road grade is an important factor for walking and cycling speeds and routes. Furthermore, enhancing real-time GPS data streams with accurate road grades would enable precise estimation of energy consumption for pedestrian or bicycle route guidance (Mendes et al., 2015) or advanced electric bicycle control (Sweeney et al., 2018). Beyond active travel, more accurate road grade information will improve energy, fuel, and emissions-sensitive vehicle routing and control algorithms for eco-driving applications and autonomous vehicles (Ma et al., 2019; Miao et al., 2018; Zeng and Wang, 2018).

One limitation of the present study is the limited number of validation sites. The quantity of 8 sites is on scale with a similar recent study that surveyed 7 locations for validation (Liu et al., 2018), but not exhaustive. Our locations were selected to capture a variety of contexts, and were not meant to be random or representative of the entire network. These are likely challenging locations for road grade estimates, and network-wide road grade estimates based on DEM will be more accurate, as the errors on elevated structures are diluted by more accurate estimates on surface streets. Another limitation is the use of single state-of-the-art methods for extraction of elevations from LIDAR data and smoothing elevations from DEM. A further examination and comparison of alternative methods is warranted, but out of scope of this study.

Future research could examination the effects of grade error on walking energy, in addition to the cycling energy calculated here. In addition, further research could be undertaken to estimate elevation profiles of long elevated structures based on surrounding network and DEM characteristics. Perhaps the underlying terrain profile and network topology could be used to infer grade modality. Such an endeavor would likely require a larger calibration data set than the 35 elevated roadways in Vancouver.

Given the importance of road grades to walking and cycling, and the rapid growth of GPS datasets for active travel, it is recommended to create a large public dataset of road grades to match with OSM network data. Many cities have precise road grade data which could be matched to OSM network links, and augmented with estimates from LIDAR cloud point data. The U.S. Geological Survey is releasing LIDAR cloud point data over increasingly large areas of the U.S. (U.S. Geological Survey, 2017), which will make it possible to develop an accurate national-level road grade dataset. Open and high-precision road grade data would provide broad benefits for transportation practitioners, researchers, and companies.

Acknowledgments

The authors wish to thank Amr Mohamed, Xugang Zhong, and Hossameldin Mohammed for their assistance in data collection, and Dylan Passmore and Dan Campbell at the City of Vancouver for providing LIDAR and design drawing data. This work was supported by the Natural Sciences and Engineering Research Council of Canada (NSERC); Ottawa, Canada; under Grant RGPIN-2016-04034.

Appendix A. Supplementary material

Supplementary data to this article can be found online at https://doi.org/10.1016/j.trc.2019.05.004.

References

Becker, J.J., Sandwell, D.T., Smith, W.H.F., Braud, J., Binder, B., Depner, J., Fabre, D., Factor, J., Ingalls, S., Kim, S.-H., Ladner, R., Marks, K., Nelson, S., Pharaoh, A., Trimmer, R., Von Rosenberg, J., Wallace, G., Weatherall, P., 2009. Global Bathymetry and Elevation Data at 30 arc seconds resolution: SRTM30_PLUS. Mar. Geod. 32, 355–371. https://doi.org/10.1080/01490410903297766.

Bernardi, S., Rupi, F., 2015. An analysis of bicycle travel speed and disturbances on off-street and on-street facilities. Transp. Res. Proc. 5, 82–94. https://doi.org/10.1016/j.trpro.2015.01.004.

Bigazzi, A.Y., Figliozzi, M.A., 2015. Dynamic ventilation and power output of urban bicyclists. Transport. Res. Rec.: J. Transport. Res. Board 2520, 52–60. https://doi.org/10.3141/2520-07.

Bigazzi, A.Y., Lindsey, R., 2018. A utility-based bicycle speed choice model with time and energy factors. Transportation 1–15. https://doi.org/10.1007/s11116-018-9907-2.

Boriboonsomsin, K., Barth, M., 2009. Impacts of road grade on fuel consumption and carbon dioxide emissions evidenced by use of advanced navigation systems. Transp. Res. Rec. 2139, 21–30. https://doi.org/10.3141/2139-03.

Boyko, A., Funkhouser, T., 2011. Extracting roads from dense point clouds in large scale urban environment. ISPRS J. Photogramm. Remote Sens. 66, S2–S12. https://doi.org/10.1016/j.isprsjprs.2011.09.009.

Broach, J., Dill, J., 2016. Using predicted bicyclist and pedestrian route choice to enhance mode choice models. Transport. Res. Rec.: J. Transport. Res. Board 2564, 52–59. https://doi.org/10.3141/2564-06.

Broach, J., Dill, J., Gliebe, J., 2012. Where do cyclists ride? A route choice model developed with revealed preference GPS data. Transport. Res. Part A: Policy Pract. 46, 1730–1740. https://doi.org/10.1016/j.tra.2012.07.005.

Cai, H., Rasdorf, W., 2008. Modeling road centerlines and predicting lengths in 3-D Using LIDAR point cloud and planimetric road centerline data. Comput. – Aided Civ. Infrastruct. Eng. 23, 157–173. https://doi.org/10.1111/j.1467-8667.2008.00518.x.

Casello, J.M., Usyukov, V., 2014. Modeling cyclists' route choice based on GPS data. Transp. Res. Rec. J. Transport. Res. Board 2430, 155–161. https://doi.org/10.3141/2430-16.

Choi, Y.-W., Jang, Y.W., Lee, H.J., Cho, G.-S., 2007. Heuristic Road Extraction. IEEE, pp. 338–342. 10.1109/ISITC.2007.63.

Clode, S., Kootsookos, P.J., Rottensteiner, F., 2004. The automatic extraction of roads from LIDAR data. In: The International Society for Photogrammetry and Remote Sensing's Twentieth Annual Congress. ISPRS, pp. 231–236.

DHI GRAS, 2014. EU-DEM Statistical Validation. European Environment Agency (EEA), Copenhagen.

Farr, T.G., Rosen, P.A., Caro, E., Crippen, R., Duren, R., Hensley, S., Kobrick, M., Paller, M., Rodriguez, E., Roth, L., Seal, D., Shaffer, S., Shimada, J., Umland, J., Werner, M., Oskin, M., Burbank, D., Alsdorf, D., 2007. The shuttle radar topography mission. Rev. Geophys. 45. https://doi.org/10.1029/2005RG000183.

Flügel, S., Hulleberg, N., Fyhri, A., Weber, C., Ævarsson, G., 2017. Empirical speed models for cycling in the Oslo road network. Transportation 1–25. https://doi.org/10.1007/s11116-017-9841-8.

Gadziński, J., 2018. Perspectives of the use of smartphones in travel behaviour studies: findings from a literature review and a pilot study. Transport. Res. Part C: Emerg. Technol. 88, 74–86. https://doi.org/10.1016/j.trc.2018.01.011.

Grejner-Brzezinska, D.A., 2002. Direct georeferencing at the Ohio State University: a historical perspective. Photogramm. Eng. Remote Sens. 68, 557–560.

Hall, P., York, M., 2001. On the calibration of Silverman's test for multimodality. Stat. Sin. 11, 515–536.

Hirano, A., Welch, R., Lang, H., 2003. Mapping from ASTER stereo image data: DEM validation and accuracy assessment. ISPRS J. Photogramm. Remote Sens. 57, 356–370. https://doi.org/10.1016/S0924-2716(02)00164-8.

Hu, Y., 2003. Automated extraction of digital terrain models, roads and buildings using airborne lidar data.

Huang, H., Cheng, Y., Weibel, R., 2019. Transport mode detection based on mobile phone network data: a systematic review. Transport. Res. Part C: Emerg. Technol. 101, 297–312. https://doi.org/10.1016/j.trc.2019.02.008.

Hughes, W.J., 2014. Global positioning system (GPS) standard positioning service (SPS) performance analysis report.

Jarihani, A.A., Callow, J.N., McVicar, T.R., Van Niel, T.G., Larsen, J.R., 2015. Satellite-derived Digital Elevation Model (DEM) selection, preparation and correction for hydrodynamic modelling in large, low-gradient and data-sparse catchments. J. Hydrol. 524, 489–506. https://doi.org/10.1016/j.jhydrol.2015.02.049.

Jarvis, A., Reuter, H., Nelson, A., Guevara, E., 2008. Hole-filled seamless SRTM data v4. International Centre for Tropical Agriculture (CIAT).

Kashani, A., Olsen, M., Parrish, C., Wilson, N., 2015. A Review of LIDAR radiometric processing: from ad hoc intensity correction to rigorous radiometric calibration. Sensors 15, 28099–28128. https://doi.org/10.3390/s151128099.

Zhang, Keqi, Chen, Shu-Ching, Whitman, D., Shyu, Mei-Ling, Yan, Jianhua, Zhang, Chengcui, 2003. A progressive morphological filter for removing nonground measurements from airborne LIDAR data. IEEE Trans. Geosci. Remote Sens. 41, 872–882. https://doi.org/10.1109/TGRS.2003.810682.

Kim, I., Kim, H., Bang, J., Huh, K., 2013. Development of estimation algorithms for vehicle's mass and road grade. Int. J. Automot. Technol. 14, 889–895. https://doi.org/10.1007/s12239-013-0097-9.

Knapen, L., Bellemans, T., Janssens, D., Wets, G., 2018. Likelihood-based offline map matching of GPS recordings using global trace information. Transport. Res. Part C: Emerg. Technol. 93, 13–35. https://doi.org/10.1016/j.trc.2018.05.014.

Li, J., Lee, H.J., Cho, G.S., 2008. Parallel algorithm for road points extraction from massive. LiDAR Data. IEEE 308–315. https://doi.org/10.1109/ISPA.2008.60.

Ling, Xu., Bedrick, E.J., Hanson, T., Restrepo, C., 2014. A comparison of statistical tools for identifying modality in body mass distributions. J. Data Sci. 12, 175–196.

Liu, H., Li, H., Rodgers, M.O., Guensler, R., 2018. Development of road grade data using the United States geological survey digital elevation model. Transport. Res. Part C: Emerg. Technol. 92, 243–257. https://doi.org/10.1016/j.trc.2018.05.004.

Ma, J., Hu, J., Leslie, E., Zhou, F., Huang, P., Bared, J., 2019. An eco-drive experiment on rolling terrains for fuel consumption optimization with connected automated vehicles. Transport. Res. Part C: Emerg. Technol. 100, 125–141. https://doi.org/10.1016/j.trc.2019.01.010.

Martin, J.C., Milliken, D.L., Cobb, J.E., McFadden, K.L., Coggan, A.R., 1998. Validation of a mathematical model for road cycling power. J. Appl. Biomech. 14, 276–291.

Mendes, M., Duarte, G., Baptista, P., 2015. Introducing specific power to bicycles and motorcycles: application to electric mobility. Transport. Res. Part C: Emerg. Technol. 51, 120–135. https://doi.org/10.1016/j.trc.2014.11.005.

Miao, C., Liu, H., Zhu, G.G., Chen, H., 2018. Connectivity-based optimization of vehicle route and speed for improved fuel economy. Transport. Res. Part C: Emerg. Technol. 91, 353–368. https://doi.org/10.1016/j.trc.2018.04.014.

Ministry of Natural Resources, Canada, 2014a. Canadian Digital Elevation Model.

Ministry of Natural Resources, Canada, 2014b. Canadian Digital Surface Model.

Nelson, A., Reuter, H.I., Gessler, P., 2009. DEM Production Methods and Sources. In: Developments in Soil Science. Elsevier, pp. 65–85 (Chapter 3). 10.1016/S0166-2481(08)00003-2.

Olds, T.S., Norton, K.I., Lowe, E.L., Olive, S., Reay, F., Ly, S., 1995. Modeling road-cycling performance. J. Appl. Physiol. 78, 1596–1611. https://doi.org/10.1152/jappl.1995.78.4.1596.

OpenStreetMap contributors, 2017. Planet dump [WWW Document]. < https://planet.osm.org > .

Oyama, Y., Hato, E., 2018. Link-based measurement model to estimate route choice parameters in urban pedestrian networks. Transport. Res. Part C: Emerg. Technol. 93, 62–78. https://doi.org/10.1016/j.trc.2018.05.013.

Parkin, J., Rotheram, J., 2010. Design speeds and acceleration characteristics of bicycle traffic for use in planning, design and appraisal. Transp. Policy 17, 335–341. https://doi.org/10.1016/j.tranpol.2010.03.001.
Payne, K.C., Dror, M., 2017. The Development of a Smart Map for Minimum "Exertion" Routing Applications. 10.24251/HICSS.2017.142.
Press, W.H. (Ed.), 1992. Numerical recipes in C: the art of scientific computing, second ed. Cambridge University Press, Cambridge ; New York.
Rodríguez, E., Morris, C.S., Belz, J.E., 2006. A global assessment of the SRTM performance. Photogramm. Eng. Remote Sens. 72, 249–260. https://doi.org/10.14358/PERS.72.3.249.
Sahlholm, P., Henrik Johansson, K., 2010. Road grade estimation for look-ahead vehicle control using multiple measurement runs. Control Eng. Pract. 18, 1328–1341. https://doi.org/10.1016/j.conengprac.2009.09.007.
Savitzky, Abraham, Golay, M.J.E., 1964. Smoothing and differentiation of data by simplified least squares procedures. Anal. Chem. 36, 1627–1639. https://doi.org/10.1021/ac60214a047.
Scholz, F.W., 2006. Maximum likelihood estimation. In: Kotz, S., Read, C.B., Balakrishnan, N., Vidakovic, B., Johnson, N.L. (Eds.), Encyclopedia of Statistical Sciences. John Wiley & Sons Inc, Hoboken, NJ, USA. https://doi.org/10.1002/0471667196.ess1571.pub2.
Silverman, B.W., 1981. Using kernel density estimates to investigate multimodality. J. Roy. Stat. Soc.: Ser. B (Methodol.) 43, 97–99.
Slater, J.A., Heady, B., Kroenung, G., Curtis, W., Haase, J., Hoegemann, D., Shockley, C., Tracy, K., 2011. Global assessment of the new ASTER global digital elevation model. Photogramm. Eng. Remote Sens. 77, 335–349. https://doi.org/10.14358/PERS.77.4.335.
Souleyrette, R., Hallmark, S., Pattnaik, S., O'Brien, M., Veneziano, D., 2003. Grade and cross slope estimation from LiDAR-based surface models.
Sweeney, S., Ordóñez-Hurtado, R., Pilla, F., Russo, G., Timoney, D., Shorten, R., 2018. A context-aware E-bike system to reduce pollution inhalation while cycling. IEEE Trans. Intell. Transp. Syst. 1–12. https://doi.org/10.1109/TITS.2018.2825436.
Tachikawa, T., Hato, M., Kaku, M., Iwasaki, A., 2011. Characteristics of ASTER GDEM version 2. IEEE, pp. 3657–3660. 10.1109/IGARSS.2011.6050017.
Tengattini, S., Bigazzi, A.Y., 2018. Physical characteristics and resistance parameters of typical urban cyclists. J. Sports Sci. 36, 2383–2391. https://doi.org/10.1080/02640414.2018.1458587.
Tengattini, S., Bigazzi, A.Y., 2017. Context-sensitive, first-principles approach to bicycle speed estimation. IET Intel. Transport Syst. 11, 411–416. https://doi.org/10.1049/iet-its.2017.0012.
Teschke, K., Chinn, A., Brauer, M., 2017. Proximity to four bikeway types and neighbourhood-level cycling mode share of male and female commuters. J. Transp. Land Use 10. https://doi.org/10.5198/jtlu.2017.943.
The City of Vancouver, 2013. LiDAR 2013 - Open Data [WWW Document]. < http://data.vancouver.ca/datacatalogue/LiDAR2013.htm > (accessed 4.3.18).
Altenhoff, Tyson, 2017. MASCOT - Management of Survey Control Operations and Tasks [WWW Document]. < http://a100.gov.bc.ca/pub/mascotw/ > (accessed 4.22.18).
UK Environment Agency, 2019. LIDAR Composite DSM - 50cm. London, UK.
U.S. Geological Survey, 2017. Lidar Point Cloud - USGS National Map 3DEP Downloadable Data Collection. Reston, VA.
U.S. Geological Survey, 2015. USGS National Elevation Dataset (NED) 1/3 arc-second Downloadable Data Collection from The National Map 3D Elevation Program (3DEP) - National Geospatial Data Asset (NGDA) National Elevation Data Set (NED). Reston, VA.
Wang, Yinsong, Zou, Y., Henrickson, K., Wang, Yinhai, Tang, J., Park, B.-J., 2017. Google Earth elevation data extraction and accuracy assessment for transportation applications. PLoS ONE 12, e0175756. https://doi.org/10.1371/journal.pone.0175756.
Willis, D.P., Manaugh, K., El-Geneidy, A., 2015. Cycling under influence: summarizing the influence of perceptions, attitudes, habits, and social environments on cycling for transportation. Int. J. Sustain. Transport. 9, 565–579. https://doi.org/10.1080/15568318.2013.827285.
Wilson, J.P., 2012. Digital terrain modeling. Geomorphology 137, 107–121. https://doi.org/10.1016/j.geomorph.2011.03.012.
Wood, E., Burton, E., Duran, A., Gonder, J., 2014. Appending High-Resolution Elevation Data to GPS Speed Traces for Vehicle Energy Modeling and Simulation. National Renewable Energy Laboratory (NREL), Golden, CO.
Zeng, X., Wang, J., 2018. Globally energy-optimal speed planning for road vehicles on a given route. Transport. Res. Part C: Emerg. Technol. 93, 148–160. https://doi.org/10.1016/j.trc.2018.05.027.
Zhang, K., Frey, H.C., 2006. Road grade estimation for on-road vehicle emissions modeling using light detection and ranging data. J. Air Waste Manag. Assoc. 56, 777–788. https://doi.org/10.1080/10473289.2006.10464500.
Ziemke, D., Metzler, S., Nagel, K., 2017. Modeling bicycle traffic in an agent-based transport simulation. Procedia Comput. Sci. 109, 923–928. https://doi.org/10.1016/j.procs.2017.05.424.